

A Two-Step Formulation of Maxwell's Equations Using Generalized Tree-Cotree Gauges for Low-Frequency-Stability

Leon Herles¹, Mario Mally^{1,2}, Jörg Ostrowski³, and Sebastian Schöps¹, Melina Merkel¹

¹Computational Electromagnetics Group, Technische Universität Darmstadt, 64289 Darmstadt, Germany

²Department of Applied Mathematics, Universidade de Santiago de Compostela, 15782, Santiago de Compostela, Spain

³Siemens Digital Industries Software, Switzerland

This paper presents a new low-frequency stabilization for a two-step formulation solving the full set of Maxwell's equations. The formulation is based on a electric scalar and magnetic vector potential equation using the electroquasistatic problem as gauge condition. The proposed stabilization technique consists of an adequate frequency scaling for the electroquasistatic problem, and a tree-cotree decomposition of the magnetic vector potential such that its divergence remains consistent with the partial decoupling of the magnetic and electric potentials. The paper discusses two variants and demonstrates the effectiveness by a few computational examples.

Index Terms—Computational Electromagnetics, Electromagnetic induction, Frequency, Maxwell equations

I. INTRODUCTION

MANY applications require accurate simulation results of electromagnetic devices over a wide frequency range, e.g., to access electromagnetic compatibility. This commonly includes static, low frequency and high frequency regimes. In such cases, static or quasi-static approximations are insufficient to capture the full functionality of the device. Therefore, we focus here on formulations that consistently solve the complete set of Maxwell's equations, allowing the evaluation of a device in both the low and high frequency regimes.

A popular starting point is the electric field formulation, e.g. [1, Section 1.2.1]. Its finite element discretization is straightforward and leads to symmetric linear systems of equations. However, the condition number of such systems tends to infinity as the frequency tends to zero, see [2]. Various approaches have been proposed, all of which decompose the field, typically based on a tree-cotree decomposition [3], [4], and its governing equations to maintain control in the frequency limit. They either start directly from the electric field or decompose it into the magnetic vector potential and the electric scalar potential first, see e.g. [5], [6], [7], [8], [9]. The main differences are in the treatment of lossy materials, the symmetry and the conditioning of the linear system as well as the number of degrees of freedom, e.g., how many Lagrange multipliers are introduced.

In this contribution we investigate the two-step formulation of Maxwell's equations originally proposed in [10]. It decouples fields and equations on the continuous level such that existing solvers can be reused when considering adequate source terms. However, we reconsider its low-frequency stability and propose a novel tree-cotree decomposition strategy.

The paper is structured as follows. In Sec. II the two-step formulation is recapitulated and discretized in Sec. III. Sec. IV discusses low-frequency stabilization techniques and their application to the two-step method. Then, Sec. V shows

the results of a numerical reference implementation. The paper closes with conclusions in Sec. VI.

II. FORMULATION

Let us consider the two-step approach from [10] in frequency domain, i.e.,

$$-\operatorname{div}(\kappa \operatorname{grad} \varphi) = i\omega \varrho^s \quad (1)$$

$$\operatorname{curl}(\nu \operatorname{curl} \mathbf{A}) + i\omega \kappa \mathbf{A} = \mathbf{J}^s - \kappa \operatorname{grad} \varphi \quad (2)$$

in its strong form on a bounded, open and simply-connected domain $\Omega \subset \mathbb{R}^3$. In (1), one solves an electroquasistatic (EQS) problem with given charge density ϱ^s , electric scalar potential φ and the complex conductivity $\kappa = \sigma + i\omega\epsilon$ which depends on angular frequency $\omega = 2\pi f$, with f being the ordinary frequency, conductivity $\sigma \geq 0$ and permittivity $\epsilon > 0$. The solution to (1) is then used to compute the right-hand-side of (2) which consists of an electricquasistatic source term $-\kappa \operatorname{grad} \varphi$ and eventually a source current density,

$$\mathbf{J}^s = \mathbf{J}_0^s + i\omega \mathbf{D}_e^s \quad \text{s.t.} \quad \operatorname{div} \mathbf{J}_0^s = 0 \quad \text{and} \quad \operatorname{div} \mathbf{D}_e^s = -\varrho^s. \quad (3)$$

The magnetic vector potential \mathbf{A} solves (2) where $\nu > 0$ denotes the reluctivity. Typical fields of interest are the magnetic flux density $\mathbf{B} = \operatorname{curl} \mathbf{A}$, the electric displacement field

$$\mathbf{D} = \epsilon \mathbf{E} = \underbrace{(-\epsilon \operatorname{grad} \varphi)}_{=\mathbf{D}_e} + \underbrace{(-i\omega\epsilon \mathbf{A})}_{=\mathbf{D}_m} + \mathbf{D}_e^s$$

and the current density

$$\mathbf{J} = \sigma \mathbf{E} = \underbrace{(-\sigma \operatorname{grad} \varphi)}_{=\mathbf{J}_e} + \underbrace{(-i\omega\sigma \mathbf{A})}_{=\mathbf{J}_m} + \mathbf{J}^s,$$

where electroquasistatic contributions are indicated by subscript e, and full-Maxwell corrections by subscript m. The conductivity σ vanishes in the nonconducting (air) region denoted by $\Omega_A \subset \Omega$; its support is denoted by $\Omega_C \subset \Omega$. Let Γ be the interface between both regions. Furthermore, we require $\operatorname{supp}(\mathbf{J}^s) \subset \Omega_A$ as well as $\operatorname{supp}(\varrho^s) \subset \Omega_A$ for the respective excitations.

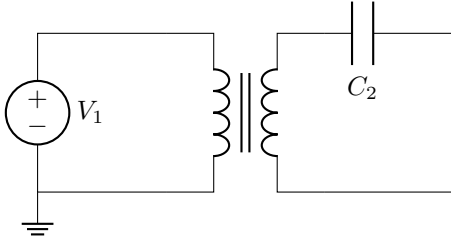


Fig. 1: Example configuration where capacitive and inductive effects are separate but must be considered simultaneously

Appropriate boundary conditions need to be provided to obtain a well-posed problem. In this work, we use combinations of homogeneous Dirichlet ($\varphi = 0$; $\mathbf{A} \times \mathbf{n} = \mathbf{0}$) and homogeneous Neumann ($\partial\varphi/\partial\mathbf{n} = 0$; $\text{curl } \mathbf{A} \times \mathbf{n} = \mathbf{0}$) boundary conditions (BCs). For imposing inhomogeneous Dirichlet BCs the usual approaches can be used [11, A2].

A. Inductive Coupling

The two-step formulation is a reformulation of the full set of Maxwell's equations and therefore includes all electromagnetic effects. Nonetheless, the decomposition into potentials may lead to counter-intuitive situations. Let us consider the field model of a series connection of a transformer and a capacitor, visualized as a circuit in Fig. 1. Let us further assume that the model is excited by $V_1 = \sin(2\pi ft)V$. Then, the electroquasistatic solution of (1) will yield a current flow and the left leg of the transformer but not through the right one since the inductive coupling is not yet considered. Consequently, the electric field and displacement currents due to C_2 will only be visible after solving (2). This requires the correction term \mathbf{D}_m of the displacement field, which would not be present in Darwin formulations [12].

This example demonstrates that one shall not attribute capacitive effects to one of the two equations or potentials alone (while this works for inductive effects). Consequently, one must always solve both equations, even if one is possibly interested in capacitive behavior only.

B. Low-Frequency Breakdown

It is clear that neither (1) nor (2) are uniquely solvable in the static limit $\omega = 0$. The electroquasistatic problem (1) degenerates into a stationary current flow problem but includes non-conductive domains [13]. On the other hand, (2) suffers from the usual non-uniqueness of the curl operators also known from the electric field formulation [2] and Darwin formulation [14], i.e., gradient fields can be arbitrarily added to the solution. This causes the low-frequency breakdown when numerically solving the problem.

III. DISCRETIZATION

Following [10], we employ the weak formulation: Find $\varphi \in H^1(\Omega)$ and $\mathbf{A} \in H(\Omega; \text{curl})$ such that

$$\int_{\Omega} (\kappa \text{grad } \varphi) \cdot \text{grad } \overline{\varphi'} dV = i\omega \int_{\Omega} \varrho^s \overline{\varphi'} dV \quad (4)$$

for all $\varphi' \in H^1(\Omega)$ and

$$\begin{aligned} \int_{\Omega} (\nu \text{curl } \mathbf{A}) \cdot \text{curl } \overline{\mathbf{A}'} + i\omega\kappa \mathbf{A} \cdot \overline{\mathbf{A}'} dV \\ = \int_{\Omega} (\mathbf{J}^s - \kappa \text{grad } \varphi) \cdot \overline{\mathbf{A}'} dV \end{aligned} \quad (5)$$

for all $\mathbf{A}' \in H(\Omega; \text{curl})$. The spaces $H^1(\Omega)$ and $H(\Omega; \text{curl})$ must be endowed with the respective BCs for which we assume that they are chosen such that (4)-(5) is well-posed.

A. Matrices and Block Structures

We follow the usual Galerkin approach. Testing and approximating equations (4)-(5) and potentials with the same basis functions from finite (sub-)spaces, i.e., $v \in V \subset H^1(\Omega)$ and $\mathbf{w} \in W \subset H(\Omega; \text{curl})$. This leads to the matrices

$$(\mathbf{K}_{\star})_{ij} = \int_{\Omega} \star(\text{grad } v_j) \cdot (\text{grad } v_i) dV, \quad (6)$$

$$(\mathbf{G}_{\star})_{ij} = \int_{\Omega} \star(\text{grad } v_j) \cdot \mathbf{w}_i dV, \quad (7)$$

$$(\mathbf{M}_{\star})_{ij} = \int_{\Omega} \star \mathbf{w}_j \cdot \mathbf{w}_i dV, \quad (8)$$

where $\star \in \{\sigma, \epsilon, \kappa\}$ denotes the employed material and the curl-curl matrix

$$(\mathbf{K}_{\nu})_{ij} = \int_{\Omega} \nu(\text{curl } \mathbf{w}_j) \cdot (\text{curl } \mathbf{w}_i) dV. \quad (9)$$

Together they form the linear equation system

$$\mathbf{K}_{\kappa} \mathbf{u} = i\omega \mathbf{q}_s \quad (10)$$

$$\mathbf{W} \mathbf{a} = \mathbf{j}(\mathbf{u}) \quad (11)$$

with $\mathbf{W} = \mathbf{K}_{\nu} + i\omega \mathbf{M}_{\kappa}$ and $\mathbf{j}(\mathbf{u}) = \mathbf{j}_s - \mathbf{G}_{\kappa} \mathbf{u}$. The degrees of freedom (DOFs) of the scalar and vector potential are given as $\mathbf{u} \in \mathbb{C}^{n_v}$ and $\mathbf{a} \in \mathbb{C}^{n_w}$, respectively. The source contributions \mathbf{q}_s and \mathbf{j}_s are constructed as

$$(\mathbf{q}_s)_i = \int_{\Omega} \varrho^s v_i dV,$$

$$(\mathbf{j}_s)_i = \int_{\Omega} \mathbf{J}^s \cdot \mathbf{w}_i dV.$$

The discrete spaces V and W have to satisfy the usual properties of nodal and edge element spaces. An interested reader is referred to [1]. Here, we chose the spaces based on multipatch isogeometric analysis (IGA) as introduced in [15]. Let us define the two index sets, cf. [13]

$$\mathcal{I}_v^{(A)} = \{1 \leq n \leq n_v \mid \text{supp}(v_n) \cap \Omega_C = \emptyset, v_n \in V\} \quad (12)$$

$$\mathcal{I}_v^{(C)} = \{1 \leq n \leq n_v \mid n \notin \mathcal{I}_v^{(A)}\} \quad (13)$$

which decompose the finite set of nodal basis functions into the ones supported only in the nonconducting domain and the others (with at least partial support in the conductor). We define $\mathcal{I}_w^{(A)}$ and $\mathcal{I}_w^{(C)}$ analogously for the edge functions. This gives rise to a block matrix partitioning, in particular

$$\mathbf{M}_{\kappa} = \begin{bmatrix} \mathbf{M}_{\sigma}^{(CC)} & \mathbf{0} \\ \mathbf{0} & \mathbf{0} \end{bmatrix} + i\omega \begin{bmatrix} \mathbf{M}_{\epsilon}^{(CC)} & \mathbf{M}_{\epsilon}^{(CA)} \\ \mathbf{M}_{\epsilon}^{(AC)} & \mathbf{M}_{\epsilon}^{(AA)} \end{bmatrix} \quad (14)$$

where $\mathbf{M}_{\sigma}^{(CC)}$ is (symmetric) positive definite while all other blocks of \mathbf{M}_{σ} vanish due to $\sigma = 0$ in Ω_A .

B. Low-Frequency Breakdown on Matrix Level

For small ω , i.e., for $\omega \rightarrow 0$, the strong formulation (1)-(2) and consequently its discretization (10)-(11) suffer from a low-frequency breakdown. For (10), this becomes obvious when examining

$$\mathbf{K}_\kappa = \begin{bmatrix} \mathbf{K}_\sigma^{(CC)} + i\omega\mathbf{K}_\epsilon^{(CC)} & i\omega\mathbf{K}_\epsilon^{(CA)} \\ i\omega\mathbf{K}_\epsilon^{(AC)} & i\omega\mathbf{K}_\epsilon^{(AA)} \end{bmatrix}, \quad (15)$$

which is singular for $\omega = 0$. This also implies that the conditioning deteriorates with decreasing ω . The ratio $\frac{\sigma}{\epsilon} \gg 1$ in Ω_C increases this issue even further. Effective modifications are proposed in [13] to improve the condition number. The focus of our paper is the stabilization of (11) which can be written as

$$\mathbf{W} = \mathbf{K}_\nu - \begin{bmatrix} \omega^2\mathbf{M}_\epsilon^{(CC)} - i\omega\mathbf{M}_\sigma^{(CC)} & \omega^2\mathbf{M}_\epsilon^{(CA)} \\ \omega^2\mathbf{M}_\epsilon^{(AC)} & \omega^2\mathbf{M}_\epsilon^{(AA)} \end{bmatrix}. \quad (16)$$

Here, the contributions from $i\mathbf{M}_\kappa$ vanish for $\omega = 0$ and only the singular \mathbf{K}_ν remains. Its kernel consists of discrete gradient fields, and additional issues arise because of large scaling differences due to $\omega\sigma \gg \omega^2\epsilon$ for $\omega \rightarrow 0$.

IV. LOW-FREQUENCY STABILIZATION TECHNIQUES

In order to combat this low-frequency breakdown, we need to recover the generalized Coulomb gauge that has been implicitly enforced by considering the two-step approach (1) and (2). It becomes evident in the strong form when a divergence is applied to (2) and divide by $i\omega$, yielding the implicit constraint

$$\text{div}(\kappa\mathbf{A}) = 0, \quad (17)$$

where we exploited that $\text{div}(\mathbf{J}^s - \kappa \text{grad} \varphi) = 0$ due to (1) and (3). This gauge apparently vanishes inside non-conducting regions if $\omega = 0$ and numerically already deteriorates in the discrete setting if ω approaches zero [10].

This motivates us to split (17) into

$$\begin{cases} \beta \text{div}((\sigma + i\omega\epsilon)\mathbf{A}) = 0 & \text{in } \Omega_C \\ \gamma \text{div}(\epsilon\mathbf{A}) = 0 & \text{in } \Omega_A \end{cases} \quad (18)$$

which has frequency-independent components in both regions. The scaling factors $\beta, \gamma \in \mathbb{R}_{>0}$ are added to further reduce the condition number but are assumed to be $\beta = \gamma = 1$ if not stated otherwise. The discrete representation of (18) is given as

$$\mathbf{S}\mathbf{a} = \begin{bmatrix} \beta \left(\mathbf{S}_\sigma^{(CC)} + i\omega\mathbf{S}_\epsilon^{(CC)} \right) & \beta\mathbf{S}_\epsilon^{(CA)} \\ \gamma\mathbf{S}_\epsilon^{(AC)} & \gamma\mathbf{S}_\epsilon^{(AA)} \end{bmatrix} \begin{bmatrix} \mathbf{a}^{(C)} \\ \mathbf{a}^{(A)} \end{bmatrix} = \mathbf{0} \quad (19)$$

with a weighted divergence matrix

$$(\mathbf{S}_\star)_{ij} = \int_{\Omega} \star \text{div}(\mathbf{w}_j) v_i \, dV \quad (20)$$

for $\star \in \{\sigma, \epsilon\}$.

By utilizing a Lagrange multiplier based approach we can include (19) in the main system (11) as

$$\begin{bmatrix} \mathbf{W} & \mathbf{S}^T \\ \mathbf{S} & \mathbf{0} \end{bmatrix} \begin{bmatrix} \mathbf{a} \\ \boldsymbol{\lambda} \end{bmatrix} = \begin{bmatrix} \mathbf{j}(\mathbf{u}) \\ \mathbf{0} \end{bmatrix}. \quad (21)$$

This increases the size of the linear system and requires the solution of a saddlepoint problem. In order to avoid the use of additional multipliers, we propose a tree-cotree based method to directly include the stabilization in the discrete problem.

A. Tree-Cotree Decomposition

To address the kernel of \mathbf{K}_ν in all of Ω , we employ a tree-cotree decomposition as described in [16], [4], [17], [9]. This approach allows us to identify which DOFs remain undetermined and which ones can be determined by only using topological mesh information. The undetermined ones correspond to edges of a spanning tree in the mesh, and we write $\mathbf{a}^{(T)}$ for the respective DOFs. The remaining (cotree) DOFs $\mathbf{a}^{(R)}$ must be determined from the magnetostatic problem

$$\begin{bmatrix} \mathbf{K}_\nu^{(RR)} & \mathbf{K}_\nu^{(RT)} \\ \mathbf{K}_\nu^{(TR)} & \mathbf{K}_\nu^{(TT)} \end{bmatrix} \begin{bmatrix} \mathbf{a}^{(R)} \\ \mathbf{a}^{(T)} \end{bmatrix} = \begin{bmatrix} \mathbf{j}^{(R)}(\mathbf{u}) \\ \mathbf{j}^{(T)}(\mathbf{u}) \end{bmatrix}. \quad (22)$$

The tree DOFs are often fixed by setting $\mathbf{a}^{(T)} = \mathbf{0}$ [16] or by prescribing a relation to the remaining DOFs [18], [4], e.g.,

$$\mathbf{a}^{(T)} = \mathbf{K}_\nu^{(TR)} \left(\mathbf{K}_\nu^{(RR)} \right)^{-1} \mathbf{a}^{(R)}. \quad (23)$$

In a second step, (22) is reformulated to compute $\mathbf{a}^{(R)}$. Note that $\mathbf{K}_\nu^{(RR)}$ has full rank, and one can show that the second row of (22) is automatically satisfied for a given $\mathbf{a}^{(T)}$ and a $\mathbf{a}^{(R)}$ that is computed from the first line of (22), see e.g. [17] or [18]. Note that we construct the tree-cotree splitting for all of Ω and also employ the following methods in both Ω_C and Ω_A .

B. Method 1: Explicit Stabilization

One can reorder the DOFs in (11) as in (22) to obtain

$$\begin{bmatrix} \mathbf{W}^{(RR)} & \mathbf{W}^{(RT)} \\ \mathbf{W}^{(TR)} & \mathbf{W}^{(TT)} \end{bmatrix} \begin{bmatrix} \mathbf{a}^{(R)} \\ \mathbf{a}^{(T)} \end{bmatrix} = \begin{bmatrix} \mathbf{j}^{(R)}(\mathbf{u}) \\ \mathbf{j}^{(T)}(\mathbf{u}) \end{bmatrix} \quad (24)$$

and show that $\mathbf{W}^{(RR)}$ has full rank, even for $\omega = 0$. The conceptual idea behind the stabilization approach is to replace the redundant (for $\omega = 0$), second line of (24) with the frequency-stable and physically consistent constraint (19). Hence, we reorder (19) to arrive at

$$\begin{bmatrix} \mathbf{S}^{(R)} & \mathbf{S}^{(T)} \end{bmatrix} \begin{bmatrix} \mathbf{a}^{(R)} \\ \mathbf{a}^{(T)} \end{bmatrix} = \mathbf{0} \quad (25)$$

and combine it with the first line of (24) to obtain

$$\begin{bmatrix} \mathbf{W}^{(RR)} & \mathbf{W}^{(RT)} \\ \mathbf{S}^{(R)} & \mathbf{S}^{(T)} \end{bmatrix} \begin{bmatrix} \mathbf{a}^{(R)} \\ \mathbf{a}^{(T)} \end{bmatrix} = \begin{bmatrix} \mathbf{j}^{(R)}(\mathbf{u}) \\ \mathbf{0} \end{bmatrix}. \quad (26)$$

C. Method 2: Schur Complement

The second approach is based on the fact that $\mathbf{S}^{(T)}$ has full rank for a specifically constructed tree and appropriate boundary conditions. This can be derived from the original idea of applying the tree-cotree splitting to the divergence operator, in [4]. Hence, one can eliminate $\mathbf{a}^{(T)}$ using a Schur complement, i.e.,

$$\mathbf{a}^{(T)} = - \left(\mathbf{S}^{(T)} \right)^{-1} \mathbf{S}^{(R)} \mathbf{a}^{(R)} \quad (27)$$

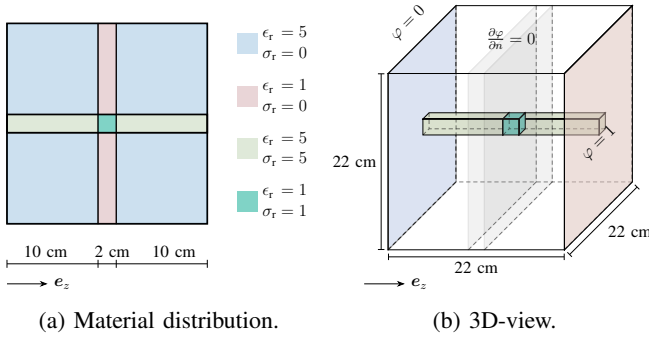


Fig. 2: Academic test example problem setup.

to arrive at

$$\left(\mathbf{W}^{(RR)} - \mathbf{W}^{(RT)} \left(\mathbf{S}^{(T)} \right)^{-1} \mathbf{S}^{(R)} \right) \mathbf{a}^{(R)} = \mathbf{j}^{(R)}(\mathbf{u}). \quad (28)$$

Consequently, the second method consists of solving (28) before inserting the result in (27) to recover $\mathbf{a}^{(T)}$. While the size of the linear system is reduced noticeably, this approach requires computing actions of $(\mathbf{S}^{(T)})^{-1}$, which may only be efficient in iterative solving procedures.

V. NUMERICAL TESTS

To evaluate the performance of the proposed stabilization method, two 3D problems are considered. The first problem is an academic example to investigate the numerical behavior of the method, while the second example deals with a more application-oriented configuration. For our numerical experiments, we employ `GeOPDES` [19] and provide the underlying implementations in [20]. There, the accuracy is controlled via the degree p of the basis functions and the number of subdivision s_h (or equivalently the element size). The scaling factors for the scaled divergence matrix (19) are chosen as

$$\beta = 1 + \omega \quad \text{and} \quad \gamma = (1 + \omega) \frac{\max_{\mathbf{x} \in \Omega} \sigma(\mathbf{x})}{\max_{\mathbf{x} \in \Omega} \varepsilon(\mathbf{x})} \quad (29)$$

to improve the condition of the system.

A. Academic Example

The first test problem consists of three conducting bars in a dielectric box. The configuration is shown in Fig. 2 and is based on the test problem of [10]. For the magnetic vector potential, we employ a homogeneous Dirichlet boundary $\mathbf{A} \times \mathbf{n} = 0$ on the whole boundary $\partial\Omega$. It is constructed such that the flux density \mathbf{D}_e does not depend on ω and is constant in space. For a more detailed derivation, see [10]. Fig. 3a shows $\|\mathbf{D}\|_2$ for $f = 0$ Hz where no frequency-dependent contributions from \mathbf{D}_m are present such that only the constant \mathbf{D}_e contributes. In Fig. 3b for $f = 100$ Hz and Fig. 3c for $f = 1000$ Hz, one can see how the resulting flux density is being pulled out of the conductor due to the correction \mathbf{D}_m .

Fig. 4 shows the condition number of the original system matrix and those of both stabilized methods. For low frequencies, the original system matrix becomes singular and thus ill-conditioned, while the condition numbers of the stabilized

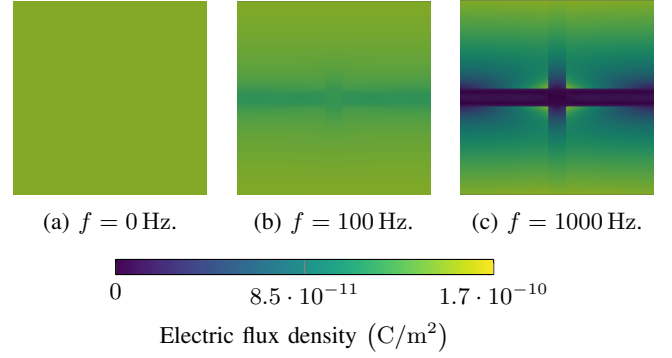
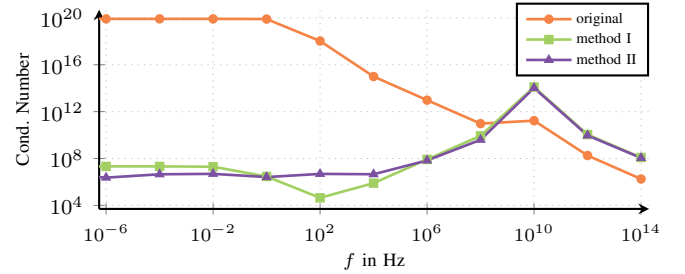
Fig. 3: Electric flux density $\|\mathbf{D}\|_2$ for different excitation frequencies.

Fig. 4: Condition number of different system matrices of academic test example over frequency.

methods stay low even for $f \rightarrow 0$. In the limit $f = 0$ Hz, we obtain condition numbers of approximately $4.87 \cdot 10^5$ and $2.34 \cdot 10^6$ for method I and II respectively, while the original system matrix is singular, as expected. For high frequencies, the condition numbers of the stabilized systems increase slightly in comparison to the one of the original. This effect is well known, see for example [21] and [4]. Fig. 5 shows the residual of the discretely evaluated generalized Coulomb gauge (17) namely

$$\delta_S = \|\mathbf{S}_\kappa \mathbf{a}\|_2 \stackrel{!}{=} 0$$

where $\|\cdot\|_2$ denotes the ℓ_2 -norm. The implicit constraint is well satisfied over the whole frequency range for both stabilized methods ($\delta_S < 1 \cdot 10^{-11}$). Even in the static limit $f = 0$ Hz, both methods remain consistent ($\delta_S = 1.52 \cdot 10^{-12}$). On the other hand, the residual of the original formulation grows significantly for small frequencies up to $\delta_S \geq 1 \cdot 10^{-2}$.

B. Simulation of Setup with Planar Coil

As a more application-motivated example, we consider a test case based on a planar coil. The problem setup is shown in Fig. 6. The copper coil has a square cross-section of $3 \text{ mm} \times 3 \text{ mm}$ and a conductivity of $\sigma = 6 \cdot 10^7 \frac{\text{S}}{\text{m}}$. It has three windings and is surrounded by air. A voltage is applied to the coil, resulting in boundary conditions $\varphi = 0$ V on Γ_G and $\varphi = (\sqrt{2})^{-1} \phi_{\text{amp}}$ on Γ_E with $\phi_{\text{amp}} = 1$ V oscillating with frequency f . On the remaining boundary $\partial\Omega \setminus (\Gamma_G \cup \Gamma_E)$, we set $\text{grad } \varphi \cdot \mathbf{n} = 0$. For the magnetic vector potential, we assume perfect magnetic boundary conditions,

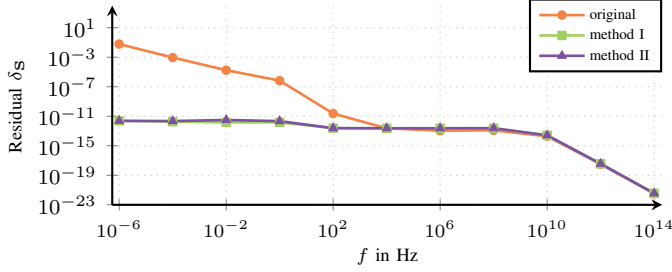


Fig. 5: Residual of discrete implicit constraint of the academic test example over frequency.

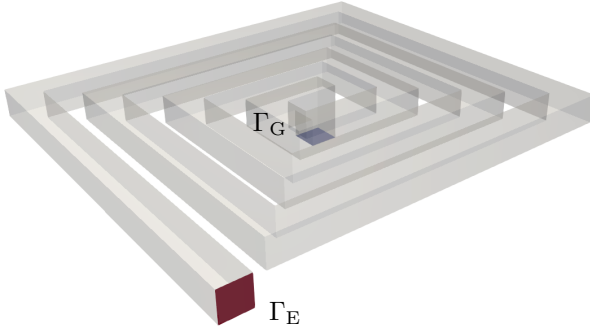


Fig. 6: Problem setup of the planar coil.

i.e., $\text{curl} \mathbf{A} \times \mathbf{n} = \mathbf{0}$. We do not impress a source current density, i.e., $\mathbf{J}^s = \mathbf{0}$.

In Fig. 7 the magnetic flux density and electric field strength are shown. The non-stable original formulation (10) and (11) does not yield correct field solutions. Note, that here, due to the large field values, the magnitude is scaled logarithmically. The stabilized versions of the two-step formulation successfully capture not only the induction of the magnetic field but also the capacitance between the coil windings correctly.

Fig. 8 shows the condition numbers of the different methods over the ordinary frequency. We can again observe that the original system becomes singular for lower frequencies. Both stabilization methods result in systems with a much lower condition number that does not deteriorate for $f \rightarrow 0$. In the static limit $f = 0\text{Hz}$, we obtain condition numbers of approximately $1.9 \cdot 10^9$ and $5.51 \cdot 10^9$ for method I and II respectively. Again, the original system matrix is singular.

C. Investigation of Inductive Coupling

We investigate the configuration sketched in Fig. 1 by utilizing again a planar coil similar to the one from the previous section. The only differences are the number of turns and that we interpret it as the left transformer leg in the context of Fig. 1. To model the right transformer leg, a conducting loop is placed above the coil. We introduce a thin slit in this upper coil with an artificially high relative permittivity of $\epsilon_r = 7.2 \cdot 10^{15}$ to model the capacitor C_2 shown in Fig. 9.

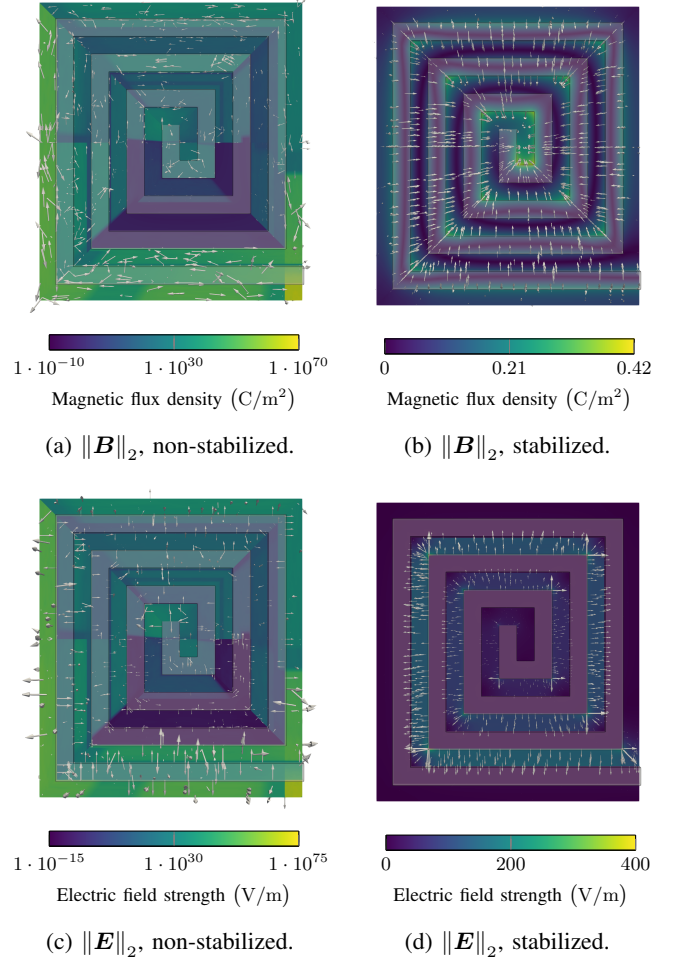


Fig. 7: Top view of the unstabilized and stabilized field solutions at $f = 150\text{Hz}$ of the planar coil, sliced in the middle. Note, that for the non-stabilized solutions the magnitudes are scaled logarithmically.

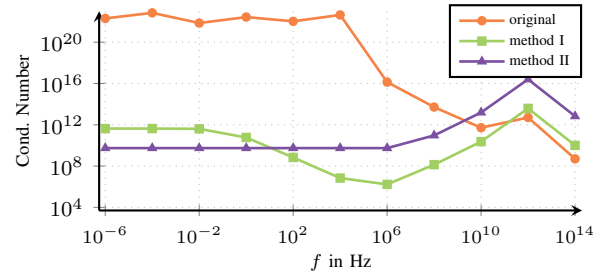


Fig. 8: Condition number of different system matrices for planar coil problem over frequency.

We employ the same boundary conditions as well as excitation as in Sec. V-B.

Fig. 9a shows the computed electric current density \mathbf{J}_e after the first step (11) of the method. Here, we can see that there is no capacitive behavior in the slit of the conductor after step 1 (as expected). Only after completing the second step, shown in Fig. 9b, the inductive coupling gives rise to a current flow in the loop and the capacitive behavior in the slit allows the electric current density $\mathbf{J} = \mathbf{J}_e + \mathbf{J}_m$ to close through the gap via $i\omega \mathbf{D}_m$. This underlines the theoretical considerations of

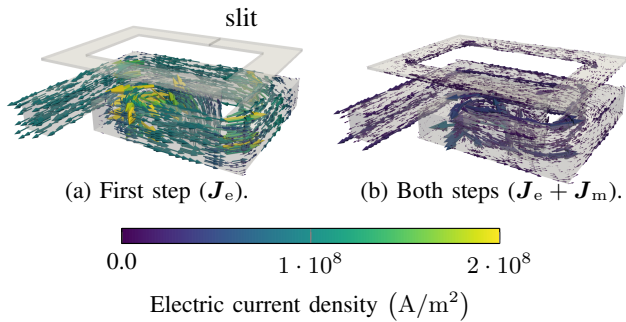


Fig. 9: Electric current density \mathbf{J} of inductively coupled problem at $f = 150$ Hz. Conductor regions are highlighted in gray and the dielectric slit in yellow.

Sec. II-A that the capacitive effect cannot be clearly attributed to either step. One can also see that the current amplitude is significantly reduced due to the inductive coupling after step 2.

VI. CONCLUSION

In this paper, we proposed a novel low-frequency stabilization approach for a two-step formulation of Maxwell's equations, leveraging a generalized tree-cotree decomposition. Our method ensures numerical stability by maintaining a consistent divergence condition for the magnetic vector potential, preventing a low-frequency breakdown. Two stabilization strategies were introduced and compared, demonstrating their effectiveness in reducing the condition number and preserving accurate field solutions across a broad frequency range including the static cases.

Through numerical experiments, we verified the proposed techniques on both academic and application-oriented test cases, confirming their robustness and efficiency. The stabilized formulation successfully captures inductive and capacitive effects simultaneously, making it a strong candidate for practical electromagnetic simulations.

ACKNOWLEDGMENT

The work is supported by the joint DFG/FWF Collaborative Research Centre CREATOR (DFG: Project-ID 492661287/TRR 361; FWF: 10.55776/F90) at TU Darmstadt, TU Graz and JKU Linz. We acknowledge the funding of The "Ernst Ludwig Mobility Grant" of the Association of Friends of Technical University of Darmstadt e.V.

REFERENCES

- [1] P. Monk, *Finite Element Methods for Maxwell's Equations*. Oxford: Oxford University Press, 2003.
- [2] J. Zhu and D. Jiao, "A theoretically rigorous full-wave finite-element-based solution of Maxwell's equations from dc to high frequencies," *IEEE Trans. Adv. Packag.*, vol. 33, no. 4, pp. 1043–1050, 11 2010.
- [3] R. Albanese and G. Rubinacci, "Magnetostatic field computations in terms of two-component vector potentials," *Int. J. Numer. Meth. Eng.*, vol. 29, no. 3, pp. 515–532, 1990.
- [4] I. Munteanu, "Tree-cotree condensation properties," *ICS Newsllett.*, vol. 9, pp. 10–14, 2002. [Online]. Available: <https://www.compumag.org/wp/newsletter/>
- [5] R. Dyczij-Edlinger, G. Peng, and J.-F. Lee, "Efficient finite element solvers for the Maxwell equations in the frequency domain," *Comput. Meth. Appl. Mech. Eng.*, vol. 169, no. 3–4, pp. 297–309, 02 1999.
- [6] R. Hiptmair, F. Kramer, and J. Ostrowski, "A robust Maxwell formulation for all frequencies," *IEEE Trans. Magn.*, vol. 44, no. 6, pp. 682–685, 06 2008.
- [7] M. T. Jochum, O. Farle, and R. Dyczij-Edlinger, "A new low-frequency stable potential formulation for the finite-element simulation of electromagnetic fields," *IEEE Trans. Magn.*, vol. 51, no. 3, p. 7402304, 03 2015.
- [8] M. Jochum, O. Farle, and R. Dyczij-Edlinger, "A symmetric and low-frequency stable potential formulation for the finite-element simulation of electromagnetic fields," in *Scientific Computing in Electrical Engineering SCEE 2014*, ser. Mathematics in Industry, no. 23. Berlin: Springer, 05 2016, pp. 63–71.
- [9] M. Eller, S. Reitzinger, S. Schöps, and S. Zaglmayr, "A symmetric low-frequency stable broadband Maxwell formulation for industrial applications," *SIAM J. Sci. Comput.*, vol. 39, no. 4, pp. B703–B731, 08 2017.
- [10] J. Ostrowski and R. Hiptmair, "Frequency-stable full Maxwell in electro-quasistatic gauge," *SIAM J. Sci. Comput.*, vol. 43, no. 4, pp. B1008–B1028, 01 2021.
- [11] L. Formaggia, F. Saleri, and A. Veneziani, *Solving Numerical PDEs: Problems, Applications, Exercises*. Springer, 2012.
- [12] M. Clemens, M.-L. Henkel, F. Kasolis, M. Günther, H. De Gerssem, and S. Schöps, "Electromagnetic quasistatic field formulations of Darwin type," *ICS Newsllett.*, vol. 29, no. 3, pp. 3–9, 03 2022, arXiv:2204.06286. [Online]. Available: <https://www.compumag.org/wp/newsletter/>
- [13] D. Balian, M. Merkel, J. Ostrowski, H. De Gerssem, and S. Schöps, "Low-frequency stabilization of dielectric simulation problems with conductors and insulators," *IEEE Trans. Dielectr. Electr. Insul.*, vol. 30, no. 6, 12 2023, arXiv:2302.00313.
- [14] H. Kaimori, T. Mifune, A. Kameari, and S. Wakao, "Low-frequency stabilized formulations of Darwin model in time-domain electromagnetic finite-element method," *IEEE Trans. Magn.*, vol. 60, no. 3, pp. 1–5, 2024.
- [15] A. Buffa, J. Rivas, G. Sangalli, and R. Vázquez Hernández, "Isogeometric discrete differential forms in three dimensions," *SIAM J. Numer. Anal.*, vol. 49, no. 2, pp. 818–844, 2011.
- [16] R. Albanese and G. Rubinacci, "Integral formulation for 3D eddy-current computation using edge elements," *IEE Proc. Sci. Meas. Tech.*, vol. 135, no. 7, pp. 457–462, 09 1988.
- [17] J. B. Manges and Z. J. Cendes, "A generalized tree-cotree gauge for magnetic field computation," *IEEE Trans. Magn.*, vol. 31, no. 3, pp. 1342–1347, 1995.
- [18] F. Rapetti, A. Alonso Rodríguez, and E. De Los Santos, "On the tree gauge in magnetostatics," *J.*, vol. 5, no. 1, pp. 52–63, 2022.
- [19] R. Vázquez, "A new design for the implementation of isogeometric analysis in Octave and Matlab: GeoPDEs 3.0," *Comput. Math. Appl.*, vol. 72, no. 3, pp. 523–554, 08 2016.
- [20] L. Herles, "LowFrequencyStableFullMaxwell," 02 2025. [Online]. Available: <https://www.doi.org/10.5281/zenodo.14810885>
- [21] R. Hiptmair, "Multilevel gauging for edge elements," *Computing*, vol. 64, no. 2, pp. 97–122, 2000.